Acta Crystallographica Section B
**Structural Science**
ISSN 0108-7681

# Electron density and atomic displacements in $KTaO_3$

**Elizabeth A. Zhurova,[a]† Yury Ivanov,[b] Valery Zavodnik[c] and Vladimir Tsirelson[b]***

[a]Chemistry Department, University of Toledo, Toledo, OH 43606, USA, [b]Mendeleev University of Chemical Technology, Moscow 125047, Russia, and [c]Karpov Institute of Physical Chemistry, ul. Vorontsovo pole 10, 103064 Moscow, Russia

† Home address: Institute of Crystallography, Russian Academy of Sciences, Moscow, Russia.

Correspondence e-mail: tsirel@muctr.edu.ru

Received 20 October 1999
Accepted 10 March 2000

The atomic interactions and anharmonicity of atomic displacements in the *virtual* ferroelectric $KTaO_3$, potassium tantalate, have been studied using accurate single-crystal X-ray diffraction at room temperature. The multipole analysis of electron density and Gram–Charlier series description of anharmonic atomic displacements allowed us to perform a quantitative analysis of the chemical bonding and atomic motion in this crystal. Closed-shell interactions between Ta—O and K—O pairs of atoms were found, while no interaction was observed for the Ta—K and O—O atomic pairs. The character of the anharmonic atomic displacements is discussed and compared with those in $SrTiO_3$.

## 1. Introduction

The displacements of ions, which are responsible for the appearance of the unit-cell dipole moment and the spontaneous polarization in ferroelectrics, depend on the nature of atomic interactions. Information regarding the anharmonicity of atomic displacements and the electron density (ED) features can be useful in choosing the phenomenological model describing the mechanism of ferroelectric phase transitions. Accurate X-ray diffraction analysis provides this information with reasonable accuracy (Tsirelson & Ozerov, 1996). Abramov, Tsirelson *et al.* (1995) demonstrated this in the recently studied $SrTiO_3$.

In this paper we report an accurate X-ray diffraction study of the atomic interactions and anharmonic atomic displacements in the cubic perovskite $KTaO_3$ (space group $Pm\bar{3}m$). It does not possess polar properties till at least 1 K, since the soft mode is stabilized by zero-point quantum fluctuations (Samara & Morosin, 1973; Axe *et al.*, 1970). Only partial substitution of K atoms by Li or Ta by Nb results in the appearance of phase transitions at low temperatures. This is the reason for $KTaO_3$ sometimes being referred to as a *virtual* or *incipient* ferroelectric.

Bussmann *et al.* (1980) highlighted two important features which should occur in ferroelectric oxides:

(i) the hybridization of oxygen 2*p* states with transition metal *d* states and

(ii) the chain-like coupling of oxygen ions to neighbouring transition metal ions.

The corresponding deformation electron density peaks were actually observed on Ti—O bonds in $SrTiO_3$ by Abramov, Tsirelson *et al.* (1995). A preliminary X-ray diffraction investigation of $K_{1-x}Li_xTaO_3$, where $x$ = 0, 0.05 and 0.15, also showed qualitatively analogous ED peaks (Zhurova *et al.*, 1995). It is interesting to explore this point in more detail.

© 2000 International Union of Crystallography
Printed in Great Britain – all rights reserved

Atomic motion and disorder in $KTaO_3$ have been previously studied by different non-diffraction methods. Salce *et al.* (1994) supposed that the soft $TO_1$ mode could be represented as the vibration of the rigid oxygen cage against Ta ions along the (100) axis. Rod *et al.* (1988) observed using NMR that even in the cubic phase with a timescale $t > 10^{-7}$ s and $T < 40$ K, the $Ta^{5+}$ ions might be in a local non-cubic environment. In the *EXAFS* study Nishihata *et al.* (1994) suggested that the anisotropy of the thermal vibration of the Ta atom in the (001) direction corresponds at low temperatures to the softening of the transverse optical phonon at the centre of a Brillouin zone. Some of these features have to result from the anharmonicity of the atomic displacements in $KTaO_3$. Indeed, in $KTaO_3$ Zhurova *et al.* (1995) observed the anharmonicity of the atomic probability density functions (p.d.f.), which are Fourier transforms of Debye–Waller factors describing the atomic displacements. Unfortunately, negative p.d.f. values in the vicinity of the O and Ta positions were found demonstrating a restricted validity of the spherical atom model used by Zhurova *et al.* (1995).

Thus, establishing the features of the chemical bond and atomic displacements in $KTaO_3$ is of great interest. To explore these properties in this work we combine a flexible analytical multipole model of the electron density and Gram–Charlier series description of anharmonic atomic displacements. This allowed us to study the atomic interactions in the crystal in terms of both the static model deformation ED maps and Bader's (1990) topological theory, and provide a more accurate description of the atomic displacements.

## 2. Experimental

Transparent $KTaO_3$ samples were grown by the spontaneous crystallization method (Syrnikov, 1990) and tested by surface emission spectroscopic analysis (Ivanov, 1992). No impurities were found within the accuracy of the method of $\sim 1\%$. Almost a perfect sphere (Table 1) with good X-ray diffraction profile shapes was chosen for the data collection at room temperature. The scan range chosen was equal to $1.2 + 0.5\tan\theta^\circ$. In order to avoid multiple scattering, an additional $\psi$ scan with 2–5° steps was applied for the low-angle reflections. A statistical precision of 1% was achieved during the measurements. The integrated intensities were obtained using profile analysis (Streltsov & Zavodnik, 1989). The reflection intensities were corrected for Lorentz and polarization factors, absorption and thermal diffuse scattering (TDS) in the two-phonon approximation (Tsarkov & Tsirelson, 1991) using elastic constants from Perry *et al.* (1989). The maximal TDS correction did not exceed 1%. Other experimental details are given in Table 1.

## 3. Refinement and results

The structural model used for the treatment of the experimental data was as follows. The electron density is approximated in the Hansen & Coppens (1978) multipole model as a sum of the atomic electron densities in the form

$$\rho_{\rm at}(\mathbf{r}) = \rho_c(r) + P_v\kappa'^3\rho_{\rm val}(\kappa' r) + \sum_{l=1}^{4}\kappa''^3 R_l(\kappa'' r)\sum_{m=-1}^{l} P_{lm}y_{lm}(\mathbf{r}/r),$$

where subscripts 'at', '*c*' and 'val' represent atomic, core and valence, respectively. The symmetry of K and Ta atom positions is $m\bar{3}m$, while O is sited in the 4/*mmm* position. Correspondingly, only a limited number of multipole parameters are different from zero. The optimized parameters were the scale factor, atomic valence-shell contraction/expansion parameters $\kappa$ and $\kappa'$, and the multipole electron populations $P_v$ and $P_{lm}$ up to hexadecapole level ($l_{\rm max} = 4$). The neutral atom wavefunctions by Clementi & Roetti (1974) for K and O, and by McLean & McLean (1981) for Ta were used to describe the core and valence electron densities. The exponential-type radial functions $r^{n_l}\exp(-\kappa'\xi r)$, with $n_l = 4, 4, 6, 8$ (K), $n_l = 6, 6, 8, 10$ (Ta) and $n_l = 2, 2, 3, 4$ (O), and values of the orbital exponents $\xi_{\rm K} = 6.0$, $\xi_{\rm Ta} = 5.35$ and $\xi_{\rm O} = 4.5$ were used. For the Ta atom this set was found empirically. Anomalous dispersion corrections were taken from *International Tables for Crystallography* (1995). The unit-cell electroneutrality condition was imposed during a multipole refinement. The isotropic secondary extinction (crystal type II) according to Becker & Coppens (1974) was chosen to minimize the *R* factor.

The anharmonicity of the atomic displacements was modelled using a Gram–Charlier expansion of the probability density function for atomic displacements up to tensors of fourth-rank (*International Tables for Crystallography*, 1995)

$$p_\mu^{\rm GC}(\mathbf{r}) = p_\mu^{\rm harm}(\mathbf{r})\{1 + (1/4!)d^{pqrs}H_{pqrs}(\mathbf{r})\},$$

where $\mathbf{r}$ is the displacement vector of an atom from its equilibrium position, $H_{pqrs}(\mathbf{r})$ is the Hermite polynomial of fourth order and $d^{pqrs}$ are anharmonic refined parameters (the third-order cumulants $c^{pqr}$ are zero for $m\bar{3}m$ and 4/*mmm* atomic sites).

Refinements were carried out using the *MOLDOS*97 program (Protas, 1997), based on the program *MOLLY* (Hansen & Coppens, 1978). The procedure of the structural model refinement, which allowed us to approximately separate the electron density asphericity and the anharmonicity of the atomic displacement, was as follows. First, the scale factor, extinction parameter, and harmonic and anharmonic atomic displacement parameters were refined using all reflections. The initial atomic valence electron populations $P_v$ were fixed to the values obtained by Zhurova *et al.* (1995), according to Hirshfeld (1977): K +0.28, Ta +0.62, O −0.30 e. All displacement parameters were then refined using reflections with $\sin\theta/\lambda \geq 0.9$ Å$^{-1}$ and fixed. Second, the scale factor, extinction parameter and the $\kappa'$, $\kappa''P_v$ and $P_{lm}$ parameters were refined using all reflections. Special attention was paid to the control of correlations between the refined parameters and the highly correlated ones were refined in separate groups. Therefore, no correlation coefficients greater than 0.7 were observed. The correctness of the final results was checked using the test from Abrahams & Keve (1971). The lowest extinction factors, observed for the (200), (110), (220) and (100) reflections, were:

$y_{min}$ = 0.68, 073, 0.78 and 0.79 ($I_{obs} = y_{min} I_{kin}$, where $I_{obs}$ and $I_{kin}$ are the observed and kinematic intensities). The final reliability factors are given in Table 1, the refined parameters are in Table 2, and the $F_o$ and $F_c$ structure factors have been deposited.[1]

The multipole parameters obtained were used to calculate the static model deformation electron density maps. The latter characterize the redistribution of electrons when spherical atoms form a crystal. The program *SALLY* (Hansen, 1990) was used. These maps in the (001) and (110) planes of the $KTaO_3$ unit cell containing all interatomic vectors are shown in Fig. 1.

The static model electron density was also used for the topological analysis performed using the *XPRO*98 program (Ivanov *et al.*, 1997). The critical points (CP) found in the electron density and their characteristics are listed in Table 3. The maps of the Laplacian of elctron density are presented in Fig. 2.

**Table 1**
Experimental details.

| | |
|---|---|
| Crystal data | |
| Chemical formula | $KO_3Ta$ |
| Chemical formula weight | 268.05 |
| Cell setting | Cubic |
| Space group | $Pm\bar{3}m$ |
| $a$ (Å) | 3.9883 (2) |
| $b$ (Å) | 3.9883 (2) |
| $c$ (Å) | 3.9883 (2) |
| $V$ (Å$^3$) | 63.44 (1) |
| $Z$ | 1 |
| $D_x$ (Mg m$^{-3}$) | 7.016 |
| Radiation type | Mo $K\alpha$ |
| Wavelength (Å) | 0.71069 |
| No. of reflections for cell parameters | 25 |
| $\theta$ range (°) | 22–24 |
| $\mu$ (mm$^{-1}$) | 44.68 |
| Temperature (K) | 298 |
| Crystal form | Sphere |
| Crystal radius (mm) | 0.056 (1) |
| Crystal color | Colorless |
| | |
| Data collection | |
| Diffractometer | Enraf–Nonius CAD-4 |
| Data collection method | $\omega/2\theta$ scans |
| Absorption correction | Corrections for a sphere |
| No. of measured reflections | 2183 |
| No. of independent reflections | 148 |
| No. of observed reflections | 148 |
| Criterion for observed reflections | $F > 3\sigma(F)$ |
| $R_{int}$ | 0.0200 |
| $\theta_{max}$ (°) | 64.50 |
| Range of $h$, $k$, $l$ | $-10 \rightarrow h \rightarrow 10$<br>$0 \rightarrow k \rightarrow 7$<br>$0 \rightarrow l \rightarrow 5$ |
| No. of standard reflections | 3 |
| Frequency of standard reflections | Every 100 reflections |
| | |
| Refinement | |
| Refinement on | $F$ |
| $R$ | 0.0043 |
| $wR$ | 0.0053 |
| $S$ | 1.050 |
| No. of reflections used in refinement | 148 |
| No. of parameters used | 28 |
| H-atom treatment | None |
| Weighting scheme | $w = 1/(\sigma^2 + 0.00002F^2)$ |
| $(\Delta/\sigma)_{max}$ | 0.0000 |
| $\Delta\rho_{max}$ (e Å$^{-3}$) | 0.1 |
| $\Delta\rho_{min}$ (e Å$^{-3}$) | −0.1 |
| Extinction method | Becker–Coppens type 2 |
| Extinction coefficient | 0.02085 |
| Source of atomic scattering factors | Calculated in *MOLDOS*97 using atomic wavefunctions from Clementi & Roetti (1974) and McLean & McLean (1981) |
| | |
| Computer programs | |
| Data reduction | Zucker *et al.* (1983) |
| Structure solution | Zucker *et al.* (1983) |
| Structure refinement | *MOLDOS*97 (Protas, 1997) |

## 4. Discussion

The ionic charges calculated from the refined monopole populations (Table 2) K + 0.14 (5), Ta + 0.66 (19) and O −0.27 (6) e are far from the formal charges $K^+Ta^{5+}O_3^{2-}$. They attest that the bonds in $KTaO_3$ are not simply ionic. We, however, should keep in mind that the multipole model only approximately provides a partition of the distributed electron density on atomic components. Therefore, it is preferable to consider the distribution of the electron density to characterize the atomic interactions.

The errors in the electron density distribution of cubic perovskites are mainly accumulated at the atomic positions owing to their high symmetry. The corresponding s.u.s of the electron density calculated according to Tsirelson & Ozerov (1996) are ∼7.0 e Å$^{-3}$ on the Ta position and ∼1.0 e Å$^{-3}$ on the O and K positions, while it is only 0.08 e Å$^{-3}$ in the interatomic space. The residual map calculated after the multipole refinement showed peaks of 0.6 e Å$^{-3}$ on the atomic positions and noise of −0.1 e Å$^{-3}$ in the interatomic space. Areas close to atomic positions are usually excluded from consideration owing to insufficient resolution and ignoring the cusp condition in any structural crystal model. Therefore, the value of 0.1 e Å$^{-3}$ can be taken as an estimate of the precision of electron density determination in $KTaO_3$.

The static deformation density maps in $KTaO_3$ crystal (Fig. 1) exhibit the statistically significant electron density peaks of 0.31 e A$^{-3}$ on Ta—O lines shifted towards O atoms. This observation is in agreement with the Bussmann *et al.* (1980) prediction, reflecting the chain-like coupling of Ta ions to neighbouring O ions by the overlap of corresponding *d* and *p* orbitals. No such features are observed on the K—O and K—Ta lines.

Electron density peaks of ∼0.2 e A$^{-3}$ corresponding to the potassium valence shell (Fig. 1*b*) are four times greater than those, for example, in $KNiF_3$ (Ivanov *et al.*, 1999). However, the values of $P_{40}$ and $P_{44+}$ multipole parameters responsible for these peaks are only 1.4 times greater than their s.u. Therefore, the statistical significance of these peaks is small

[1] Supplementary data for this paper are available from the IUCr electronic archives (Reference: BR0094). Services for accessing these data are described at the back of the journal.

**Table 2**
$KTaO_3$: harmonic and anharmonic displacement and multipole parameters.

The atomic coordinates are: Ta(0, 0, 0), O ($\frac{1}{2}$, 0, 0) and K ($\frac{1}{2}$, $\frac{1}{2}$, $\frac{1}{2}$)

| | K | Ta | O |
|---|---|---|---|
| $U^{11}$ | 0.0082 (2) | 0.00332 (3) | 0.0035(8) |
| $U^{22}$ | $U^{11}$ | $U^{11}$ | 0.0092 (4) |
| $d_{1111} \times 10^4$ | 0.0006 (20) | −0.0011 (2) | −0.0025 (15) |
| $d_{2222} \times 10^4$ | $d_{1111}$ | $d_{1111}$ | 0.0008 (30) |
| $d_{1122} \times 10^4$ | 0.0016 (40) | −0.0019 (4) | −0.0008 (50) |
| $d_{2233} \times 10^4$ | $d_{1122}$ | $d_{1122}$ | 0.0048 (40) |
| $\kappa'$ | 0.74 (10) | 1.48 (7) | 0.94 (1) |
| $\xi\kappa''$ | 6.0 | 4.22 (37) | 6.9 (5) |
| $P_v$ | 0.86 (5) | 4.34 (19) | 6.27 (6) |
| $P_{20}$ | – | – | 0.01 (3) |
| $P_{40}$ | 0.19 (14) | 1.08 (29) | −0.1 (3) |
| $P_{44+}$ | 0.14 (10) | 0.80 (21) | 0.006 (32) |

(note that the electron population of the K atom is statistically significant, see Table 1).

The maps of the Laplacian of the electron density revealed a large electron density concentration in the atomic basins. The Laplacian of potassium exhibits only three electron density shells: this bonded ion lacks the outer nodes found in the case of free $K^+$ ions (Bader & Essen, 1984). The outer valence minima and maxima in the Laplacian around the Ta atom are not resolved, in agreement with previous observations (Tsirelson & Ozerov, 1996).

The number of different types of critical points in the electron density listed in Table 3 obeys the Poincare–Hopf–Morse condition (Johnson, 1977; Zou & Bader, 1994; Martin Pendas *et al.*, 1997). Six (3, −1) critical points are found on Ta—O lines and 12 (3, −1) on K—O. The presence of these critical points on the interatomic lines indicates the existence of the bond between corresponding atoms (Bader, 1990). We can conclude that the geometrical and topological coordination numbers of Ta and K are the same: 6 and 12, respectively. At the same time, in spite of the fact that the nearest K—O and O—O distances are the same (2.8202 Å), oxygen is bonded to only two Ta atoms and four K atoms. Therefore, the *topological* coordination number of the O atom is only 6.

All the (3, −1) critical points in $KTaO_3$ are characterized by the positive Laplacian of the electron density values. According to Bader (1990), this is an indication of the closed-shell interaction between the corresponding atoms. However, it is clear that Ta—O and K—O bonds are different; this difference manifests itself in the value and curvature of the electron density distribution in the critical point on the interatomic lines (see Table 3). Analysing the topological characteristics available in the literature extracted from the experimental and theoretical electron density, Tsirelson (1999) found that the bonds, typically identified as ionic, are characterized by the electron density value at the (3,−1) critical point in the range 0.07–0.25 e $A^{-3}$. Another remarkable feature of these bonds is the specific range of the ratio of the perpendicular and parallel curvatures of the electron density: $0.12 < |\lambda_1|/\lambda_3 < 0.17$. The K—O interaction fits both conditions if we take $|(\lambda_1 + \lambda_2)/2|$ rather than $\lambda_1$: $|(\lambda_1 + \lambda_2)/2|/\lambda_3 \simeq 0.15$. Topological characteristics of the (3,−1) critical points on the Ta—O line listed in Table 2 and the ratio $|\lambda_1|/\lambda_3 = 0.30$ allow us to classify this bond, following Bader & Essen (1984), as an *intermediate* between closed-shell and the polar shared interactions description. The concentration of the valence electrons of O atoms in non-bonding directions (Fig. 2) with the corresponding Laplacian maxima at 0.38 Å from the atomic positions stress the dominant closed-shell nature of the Ta—O interaction.

It is worth mentioning that the deformation electron density peak on the Ta—O bond lies 1.18 Å from Ta and 0.81 Å from O, and does not mimic anharmonic smearing of the electron density. The possible correlations between multipole and anharmonic displacement parameters were avoided using the refinement procedure described above. Therefore, we can conclude that the anharmonicity of the atomic displacements and the asphericity of the valence electron distribution in Ta—

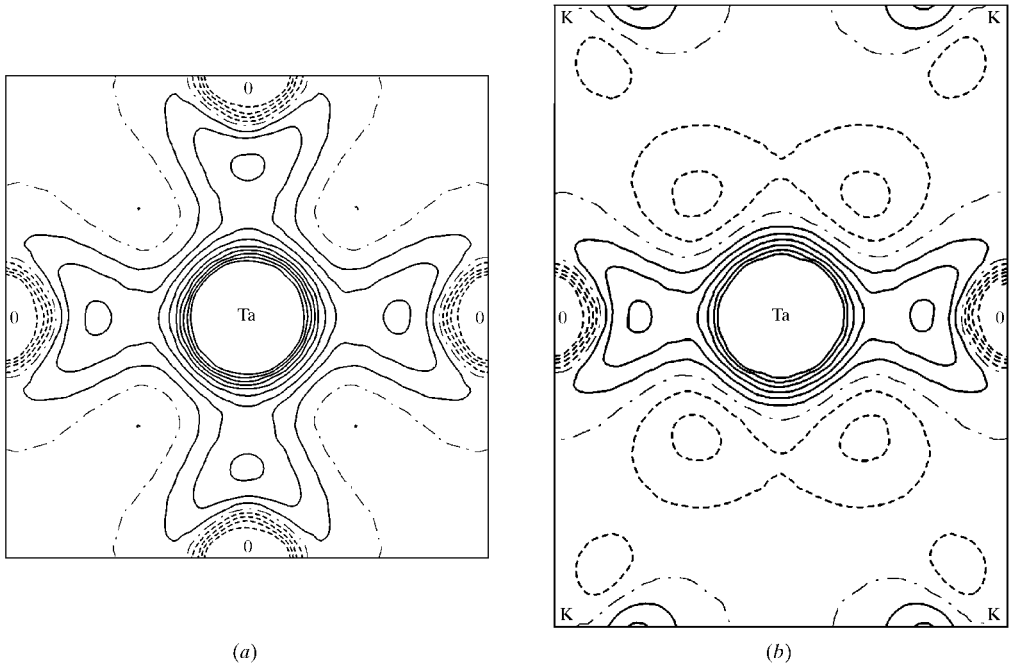


(*a*) (*b*)

**Figure 1**
Static model deformation electron density in (*a*) (001) and (*b*) (110) planes. The contour interval is 0.1 e $A^{-3}$. Positive contours are solid, negative ones are dashed and the zero level is dash–dotted. Contours in the vicinity of atomic positions are omitted.

O bonds in $KTaO_3$ are reasonably separated in the structural model.

The anharmonicity of K atom displacements is very weak and possesses no specific features. The p.d.f., $p(\mathbf{u})$, of the O atom is shown in Fig. 3. In contrast to the early consideration of Zhurova *et al.* (1995), this p.d.f. is positive in all the space around the regular position, exhibiting a splitting along the Ta—O—Ta line with a displacement of 0.066 Å. Mainly the $d_{1111}$ anharmonic parameter describes this splitting. Taking into account the s.u. of the $d_{1111}$ parameter (see Table 2), we can conclude that the statistical significance of the detection of this splitting is ∼91%. Note that the refinement of the harmonic disorder model gave a significant value of oxygen displacement of 0.06 (2) Å (Zhurova *et al.*, 1995). From the X-ray diffraction data at one temperature we cannot determine if this p.d.f. feature has static or dynamic nature.

The effective one-particle atomic displacement potential (OPP), $V(\mathbf{r})$, which is used in the phenomenological models describing the mechanism of ferroelectric phase transitions, is related to the p.d.f. $p(\mathbf{r})$ by the expression

$$V_\mu(\mathbf{r}) = -kT \ln[p_\mu(\mathbf{r})/p_\mu(\mathbf{r} = \mathbf{r}_0)],$$

where $k$ is Bolzmann's constant and $T$ is temperature (Willis, 1969). These OPPs for O and Ta atoms normalized to the maximum p.d.f. values are presented in Figs. 4 and 5. The OPP of the O atom (Fig. 4) has two minima along the Ta—O—Ta line separated by the barrier 240 meV. The OPP of the Ta atom (Fig. 5) is not defined in the small vicinity of the atomic position because the corresponding p.d.f. is negative in this region, probably owing to insufficient resolution which is

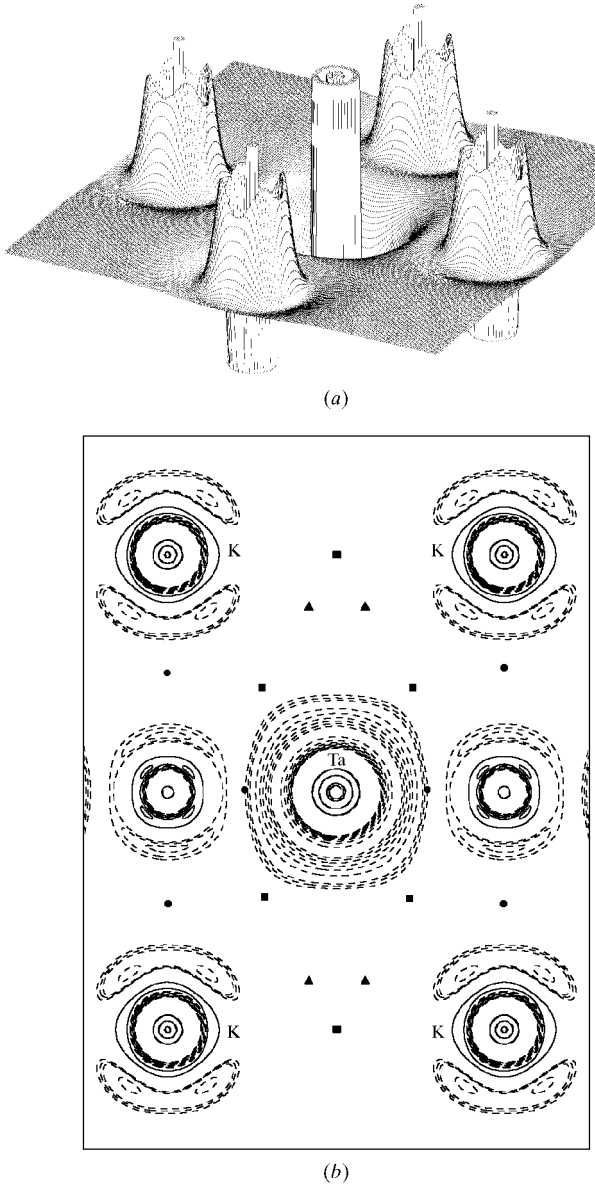


(*a*)

(*b*)

**Figure 2**
Laplacian of the electron density in $KTaO_3$: (*a*) negative Laplacian in the (001) plane and (*b*) the total Laplacian (110) plane. Contours are: 8, 9, 10, 15, 20, 25, 30 and 35 e Å$^{-5}$; the interval in the ranges 40–400 and −40 to −400 e Å$^{-5}$ is 40 e Å$^{-5}$. The solid lines depict the negative values of the Laplacian, corresponding to the concentration of the electron density; positive values are dashed. The critical points of electron density (3,−1), (3,+1) and (3,+3) are denoted by dots, triangles and squares, respectively.

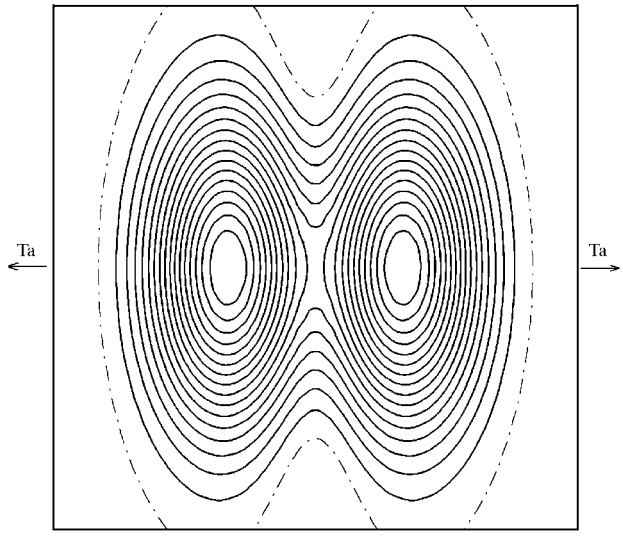


**Figure 3**
Probability density function (p.d.f.) distribution of the O-atom positions in the (001) plane; contour interval 500 Å$^{-3}$. The point ($\frac{1}{2}$00) is at the center; the dimensions are 0.4 × 0.4 Å.

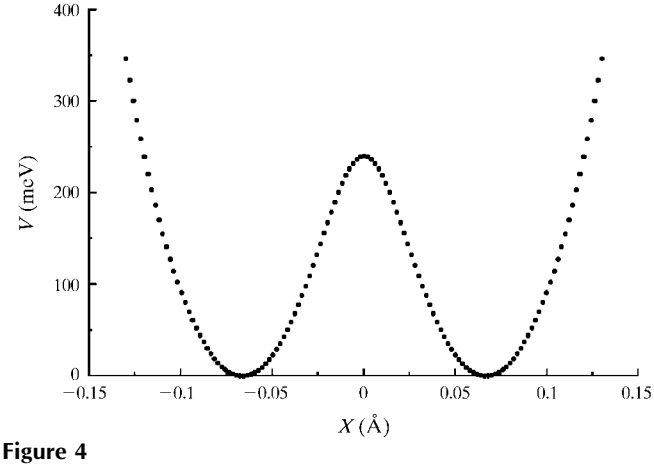


**Figure 4**
Effective one-particle potential of the O atom along the Ta—O—Ta line.

**Table 3**
Characteristics of the critical points in the $KTaO_3$ crystal.

$\nabla^2\rho(\mathbf{r}_{cp}) = \lambda_1 + \lambda_2 + \lambda_3$, where $\lambda_1$ and $\lambda_2$ are perpendicular to the bond line curvatures of the electron density and $\lambda_3$ is parallel.

| Critical point position | $\rho(\mathbf{r}_{cp})$ (e Å$^{-3}$) | $\nabla^2\rho(\mathbf{r}_{cp})$ (e Å$^{-5}$) | $\lambda_1$ (e Å$^{-5}$) | $\lambda_2$ (e Å$^{-5}$) | $\lambda_3$ (e Å$^{-5}$) | Type of critical point |
|---|---|---|---|---|---|---|
| (0.2705, 0, 0)† | 1.08 (9) | 7.90 (3) | −5.94 | −5.94 | 19.78 | (3,−1) |
| (0.2469, 0.2469, $\frac{1}{2}$)‡ | 0.08 (2) | 1.48 (1) | −0.47 | −0.15 | 2.10 | (3,−1) |
| (0.3849, 0.3849, 0.0882) | 0.03 (3) | 0.58 (2) | −0.15 | 0.28 | 0.45 | (3,+1) |
| ($\frac{1}{2}$, $\frac{1}{2}$, 0) | 0.02 (2) | 0.24 (1) | 0.06 | 0.06 | 0.12 | (3,+3) |
| (0.2227, 0.2227, 0.2227)§ | 0.00 (6) | 3.16 (2) | 0.93 | 0.93 | 1.30 | (3,+3) |

† Ta—O line. ‡ —K—O line § —Ta—K line.

important for heavy atoms. However, a general pattern is clear: OPP has a local maximum at the regular Ta atom position and six well defined minima along the Ta—O lines sited at ∼0.1 Å from this point. Note that similar behaviour of the Bi atom was observed by Abramov, Reznik *et al.* (1995) in perovskite $Ba_{0.87}K_{0.13}BiO_3$.

It is instructive to compare the character of the atomic p.d.f. in $KTaO_3$ and $SrTiO_3$ (Abramov, Tsirelson *et al.*, 1995). $SrTiO_3$ is also a *virtual* ferroelectric since it does not make a ferroelectric phase transition at any finite temperature (Jauch & Palmer, 1999). However, unlike $KTaO_3$, $SrTiO_3$ possesses an antiferrodistortive phase transition at ∼106 K, which gives rise to the tetragonal phase owing to rotations of oxygen octahedra. The oxygen p.d.f. maps for $SrTiO_3$ and $KTaO_3$ are almost identical: both exhibit a ∼0.06 Å shift of the p.d.f. maxima from the ideal positions of the O atoms. The p.d.f. of Ta differs from that of the Ti atom in $SrTiO_3$: the splitting in the Ti p.d.f. was found in the directions of the cubic face diagonals. This pattern of the atomic p.d.f. was explained by Abramov, Tsirelson *et al.* (1995). They suggested that overlapping between vacant *d* orbitals of the $Ti^{+4}$ ion and filled *p* orbitals of its $O^{2-}$ ligands results in an off-center shift of the $Ti^{4+}$ ion owing to a second-order Jahn–Teller effect. Electronic instability also leads to a displacement of the Ti and O atoms towards or away from each other in such way that some Ti—O bonds are shortened while others are lengthened. The corresponding distortion of the $TiO_6$ octahedron, modeled in terms of the bond-valence model (Brown, 1992), was found to be in excellent agreement with the positions of the p.d.f. maxima.

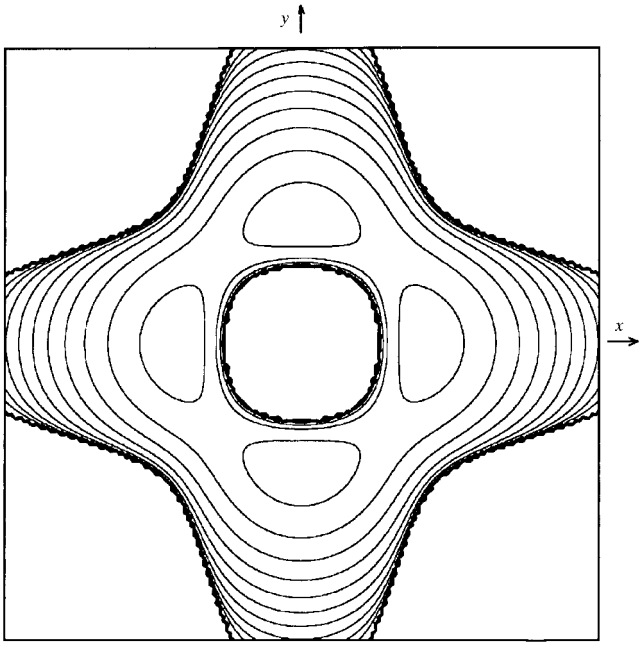


**Figure 5**
Effective one-particle potential of the Ta atom in the (001) plane, with a contour interval of 200 meV; the dimensions are 0.48 × 0.48 Å.

The general pattern of the atomic displacements in $KTaO_3$ and $SrTiO_3$ is consistent with the presence of two temperature-dependent modes: a ferroelectric soft $TO_1$ mode involving the displacements of Ta or Ti and maybe O atoms, and a ferroelastic mode involving the rotation of oxygen octahedra. Unlike $SrTiO_3$, in $KTaO_3$ the second mode weakly changes with temperature (Perry *et al.*, 1989) and the antiferrodistortive phase transition never takes place. Migoni *et al.* (1976) pointed out that the behaviour of the ferroelectric soft mode in $ABO_3$ perovskites (and related properties) can be connected to the high anisotropic deformability of the O ion, which strongly depends on its environment in a crystal. In fact, $K_{1-x}Li_xTaO_3$ crystals do exhibit the ferroelectric phase transitions at low temperatures. The X-ray diffraction investigation of $K_{1-x}Li_xTaO_3$ with $x$ = 0.05 and 0.15 at room temperature showed practically the same deformation electron density and atomic p.d.f.'s as the pure $KTaO_3$ (Zhurova *et al.*, 1995).

Kunz & Brown (1995) pointed out that the reasons for the displacement of Ta in an octahedral environment should be similar to that for Ti. Therefore, we can suggest that the explanation offered by Abramov, Tsirelson *et al.* (1995) for $SrTiO_3$ also holds for $KTaO_3$. Displacements in the directions [111], [100] and [110] are allowed by the bond-valence model, but off-center directions in which the Ti or Ta atom moves will depend on factors that we cannot yet predict.

All these facts together do mean that *virtual* ferroelectric $KTaO_3$ has qualitatively the same character of the electron density distribution and the pattern of the atomic displacements as the crystals possessing phase transitions. These features, probably, form the structural field in which other factors realise phase transitions of different types.

We thank Dr S. A. Ivanov and Dr V. V. Zhurov for the help in sample preparation and useful discussions.

## References

Abrahams, S. C. & Keve, E. T. (1971). *Acta Cryst.* A**27**, 157–165.
Abramov, Yu. A., Reznik, I. M., Tsirelson, V. G. & Okamura, F. P. (1995). *Physica C*, **254**, 189–192.

Abramov, Yu. A., Tsirelson, V. G., Zavodnik, V. E., Ivanov, S. A. & Brown, I. D. (1995). *Acta Cryst.* B**51**, 942–951.
Axe, J. D., Harada, J. & Shirane, G. (1970). *Phys. Rev. B*, **1**, 1227–1234.
Bader, R. F. W. (1990). *Atoms in Molecules – A Quantum Theory*. Oxford University Press.
Bader, R. F. W. & Essen, H. (1984). *J. Chem. Phys.* **80**, 1943–1960.
Becker, P. J. & Coppens, P. (1974). *Acta Cryst.* A**30**, 129–147.
Brown, I. D. (1992). *Acta Cryst.* B**48**, 553–572.
Bussmann, A., Bilz, H., Roenspiess, R. & Schwarz, K. (1980). *Ferroelectrics*, **25**, 343–346.
Clementi, E. & Roetti, C. (1974). *At. Data Nucl. Data Tables*, **14**, 177–478.
Hansen, N. (1990). *SALLY*. University of Nancy I, France.
Hansen, N. & Coppens, P. (1978). *Acta Cryst.* A**34**, 909–921.
Hirshfeld, F. L. (1977). *Theor. Chim. Acta*, **44**, 129–138.
Ivanov, S. A. (1992). Private communication.
Ivanov, Yu., Abramov, Yu. & Tsirelson, V. (1997). National Conference on the Application of the X-ray, Neutrons and Electrons for Study of Materials, Moscow, Dubna. Abstracts, p. 599.
Ivanov, Yu., Zhurova, E. A., Zhurov, V. V., Tanaka, K. & Tsirelson, V. G. (1999). *Acta Cryst.* B**55**, 923–930.
Jauch, W. & Palmer, A. (1999). *Phys. Rev. B*, **60**, 2961–2963.
Johnson, C. K. (1977). *Am. Crystallogr. Assoc. Winter Meeting*, Asilomar. Abstracts, p. 30.
Kunz, M. & Brown, I. D. (1995). *J Solid State Chem.* **115**, 395–406.
Martin Pendas, A. M., Costales, A. & Luana, V. (1997). *Phys. Rev. B*, **55**, 4275–4284.
McLean, A. D. & McLean, R. S. (1981). *At. Data Nucl. Data Tables*, **26**, 197–381.
Migoni, R., Bilz, H. & Bäuerle, D. (1976). *Phys. Rev. Lett.* **37**, 1155–1158.
Nishihata, Y., Kamishima, O., Ojima, K., Sawada, A., Maeda, H. & Terauchi, H. (1994). *J. Phys. Condens. Matter*, **6**, 9317–9328.
Perry, C. H., Currat, R., Migoni, R. M., Stirling, W. G. & Axe, J. D. (1989). *Phys. Rev. B*, **39**, 8666–8676.
Protas, J. (1997). *MOLDOS*96/*MOLLY*: IBM PC MS DOS Updated Version. University of Nancy I, France.
Rod, S., Borsa, F. & van der Klink, J. J. (1988). *Phys. Rev. B*, **38**, 2267–2272.
Salce, B., Gravil, J. L. & Boatner, L. A. (1994). *J. Phys. Condens. Matter*, **6**, 4077–4092.
Samara, G. A. & Morosin, B. (1973). *Phys. Rev. B*, **8**, 1256–1264.
Streltsov, V. A. & Zavodnik, V. E. (1989). *Sov. Phys. Crystallogr.* **34**, 824–828.
Syrnikov, P. P. (1990). Private communication.
Tsarkov, A. G. & Tsirelson, V. G. (1991). *Phys. Status Solidus B*, **167**, 417–428.
Tsirelson, V. G. (1999). *XVIIIth IUCr Congress and General Assembly*, 4–13 August 1999, Glasgow, Scotland. Abstract M13.OF.003.
Tsirelson, V. G. & Ozerov, R. P. (1996). *Electron Density and Bonding in Crystals*. Bristol, Philadelphia: IOP.
Willis, B. T. M. (1969). *Acta Cryst.* A**25**, 277–300.
Zhurova, E. A., Zavodnik, V. E. & Tsirelson, V. G. (1995). *Crystallogr. Rep.* **40**, 816–823.
Zou, P. F. & Bader, R. F. W. (1994). *Acta Cryst.* A**50**, 714–725.
Zucker, U. H., Parenthaler, E., Kuhs, W. F., Bachman, R. & Schulz, H. (1983). *J. Appl. Cryst.* **16**, 358.